An improved method for the synthesis of the silicoaluminophosphate molecular sieves, SAPO-5, SAPO-11 and SAPO-31

A.K. Sinha, S. Sainkar, S. Sivasanker *

National Chemical Laboratory, Pune 411 008, India

Abstract

Medium-pore molecular sieves SAPO-11 and SAPO-31 and large-pore molecular sieve SAPO-5 were synthesized using the same template (dipropylamine) by gradual heating of the synthesis gel to obtain highly crystalline materials within 1 to 2 h. This synthesis method resulted in higher acidity and better incorporation of Si^{4+} at P^{5+} sites, resulting in a lower concentration of silica islands as evidenced from ^{29}Si magic-angle spinning nuclear magnetic resonance spectroscopy. The particles of the samples synthesized by this method were more uniform in size and morphology than conventionally synthesized samples. The rapidly crystallized samples showed a higher activity and selectivity than conventionally synthesized samples in the isomerization of *m*-xylene and the alkylation of toluene. © 1999 Elsevier Science B.V. All rights reserved.

1. Introduction

Just as several organic amines are known to produce the same zeolite framework structure, cases of a single organic molecule producing different framework structures on changing the synthesis variables slightly have also been recorded [1]. For example, dipropylamine (DPA) has been used in the synthesis of many $AlPO_4$ molecular sieves with straight channels [2]. By varying the synthesis parameters, $AlPO_4$-11 (AEL), VPI-5 (VFI), $AlPO_4$-H3 (APC), MAPO-39 (ATN), CoAPO-43 (GIS), MAPSO-46 (AFS) and CoAPO-50 (AFY) have been prepared (using DPA). Even though they have different structures, they all have straight channels with at least eight-membered ring pore openings.

Wilson et al. [3,4] explained the structure-directing effects of organic amines with reference to their steric and electronic effects. In the synthesis of $AlPO_4$-11, Tapp et al. [5] indicated the role of organic bases in both electronic- and structure-directing effects. Because of the phenomenon of obtaining multiple structures from one template [4], gel chemistry becomes very important (to obtain a specific structure) because the hydrothermal crystallization of aluminophosphates is kinetically controlled and the nuclei that reach the critical size first determine the final product. The

---

* Corresponding author.
  E-mail address: siva@ems.ncl.res.in (S. Sivasanker)

desirable pH range of the hydrous gel has been found to be 3.5–6.0 for the successful crystallization of microporous aluminophosphates.

SAPO-11 has the ALPO$_4$-11 (AEL) topology, comprising unidirectional, non-intersecting, 10-membered ring channels with elliptical pore apertures of 0.63 nm × 0.39 nm. The topology consists of sheets of six-ring–six-ring–four-ring (S6R–S6R–S4R) units. SAPO-31 has AlPO$_4$-31 (ATO) topology with unidimensional, non-intersecting, 12-membered ring channels with circular pore openings and non-planar layers of alternating S4R and S6R building units. SAPO-5 has a topology of AlPO$_4$-5 (AFI) type with alternating four- and six-membered rings as secondary building units. The pore system consists of non-connecting, parallel channels of 12-membered rings. Thus, these three structures (SAPO-5, SAPO-11 and SAPO-31) seem to be related. However, even though SAPO-11 and SAPO-31 have been crystallized by using dipropylamine as the organic template, SAPO-5 has not been reported so far even as an impurity phase during the synthesis of different molecular sieves using dipropylamine.

Silicoaluminophosphate molecular sieves have acquired considerable importance as catalysts owing to their excellent selectivity towards isomerization of n-alkanes. This results from their moderate acidity compared with zeolites, which exhibit considerable cracking due to strong acidity. Pt/SAPO-11 shows a high selectivity for monobranched isomers due to catalysis at the pore mouth and hence has been found to be an excellent catalyst in the dewaxing of heavy petroleum oils [6]. Numerous studies have reported the relative activities of the SAPOs in the transformation of many n-alkanes [7–9]. Using the procedures reported by Lok et al. [10] for the synthesis of SAPO-11 results in the formation of a substantial amount of silicon-containing islands, as evidenced by ^{29}Si magic-angle spinning (MAS) nuclear magnetic resonance spectroscopy (NMR). It has been shown that the addition of silicon above an upper limit (which depends on the structure type) tends to generate siliceous islands. This increases the acid strength by forming Si(nAl) species, with $n < 4$, at the border of the islands [11]. The formation of siliceous islands in SAPOs is thermodynam-

ically favoured because it has been found that heating of SAPO molecular sieves at high temperature induces a solid-state transformation due to the mobility of atoms and isolated silicon atoms migrate to form silicon islands in the framework [12].

In this paper we report that the synthesis of SAPO-5 using DPA takes place when the synthesis gel is heated slowly at a programmed rate. Moreover, we find that SAPO-31 and SAPO-11 can also be synthesized from the same gel by varying some synthesis parameters. More importantly, programmed heating of the gel produces crystalline products more rapidly. The SAPOs so synthesized are also more active in acid-catalysed reactions (*m*-xylene isomerization and toluene alkylation) than those synthesized by conventional methods as a consequence of their better distribution of silicon.

2. Experimental

SAPO-5, SAPO-11 and SAPO-31 were crystallized hydrothermally using fumed silica (Cabosil), silica sol (28% SiO$_2$), tetraethylorthosilicate (99%; Aldrich, USA), aluminium isopropoxide (Aldrich, USA), orthophosphoric acid (85%; sd finechem, India) and dipropylamine (99%; Aldrich, USA). Stainless steel autoclaves (150 cm^3) were used for all the syntheses at autogenous pressure without agitation. The molar compositions of the reaction mixtures and the synthesis conditions for the preparation of the pure SAPOs are given in Table 1. In a typical synthesis, a slurry of aluminium isopropoxide (11.6 g) in water (13.0 g) was stirred mechanically for 45 min, orthophosphoric acid (6.4 g) diluted with water (6.5 g) was added dropwise to the stirred slurry and the stirring was continued for 1.5 h. Dipropylamine (4.2 g) and fumed silica/silica sol/TEOS were then added, and the mixture was stirred for another 2 h to get a homogenous gel. The gel was heated in an autoclave at 1.5 K min^{-1} to 433 K, then at 0.5 K min^{-1} to 473 K and the temperature was maintained for a suitable time. Other heating rates in the range from 0.5 to 3 K min^{-1} were also tried in the experiments. Use of a single heating rate

Table 1
Synthesis conditions for SAPOs (crystallization temperature = 473 K)

Experiment no.	Gel composition (molar ratio)	Crystalliztion time, t_c (h)	pH		Product	Silica source	Crystallinity (%)[a]
			Before crystallization	After crystallization			
Method 1 [conventional (s)]							
1	$Al_2O_3:1.0P_2O_5:1.0DPA:0.2SiO_2$	24	5.8	8.6	SAPO-11(s)	Fumed silica	83
2	$Al_2O_3:1.0P_2O_5:1.0DPA:0.2SiO_2$	24	6.2	8.9	SAPO-31(s)	Fumed silica	87
3	$Al_2O_3:1.0P_2O_5:1.0 EA:0.6SiO_2$	24	4.8	8.4	SAPO-5(s)	Fumed silica	92
Method 2 [rapid (r)]							
4	$Al_2O_3:1.1P_2O_5:1.5DPA:0.2SiO_2$	0	6.8	8.3	SAPO-11(r)	Fumed silica	82
		2		9.2	SAPO-11(r)	Fumed silica	100
		4		8.9	SAPO-11(r)	Fumed silica	96
		6		8.6	SAPO-11(r)	Fumed silica	91
5	$Al_2O_3:1.1P_2O_5:1.6DPA:0.2SiO_2$	2	7.4	9.5	SAPO-11 +SAPO-5	Fumed silica	na[b]
6	$Al_2O_3:1.1P_2O_5:1.5DPA:0.3SiO_2$	0	6.8	9.2	SAPO-11 +SAPO-5	Fumed silica	na
7	$Al_2O_3:1.1P_2O_5:1.5DPA:0.35SiO_2$	0	7.0	9.4	SAPO-11 +SAPO-5	Fumed silica	na
8	$Al_2O_3:1.1P_2O_5:1.5DPA:0.4SiO_2$	0	6.8	9.3	SAPO-5	Fumed silica	95
9	$Al_2O_3:1.1P_2O_5:1.5DPA:0.6SiO_2$	0	7.1	9.1	SAPO-5	Fumed silica	100
		1		9.2	SAPO-5 +SAPO-11	Fumed silica	na
		2		9.2	SAPO-5 +SAPO-11	Fumed silica	na
10	$Al_2O_3:1.1P_2O_5:1.3DPA:0.6SiO_2$	0	6.8	8.8	SAPO-5	Fumed silica	100
11	$Al_2O_3:1.1P_2O_5:1.5DPA:0.8SiO_2$	0	7.1	9.2	SAPO-5	Fumed silica	88
12	$Al_2O_3:1.1P_2O_5:1.5DPA:0.2SiO_2$	0	6.5	7.8	Lamellar	Silica sol	na
		2		8.5	SAPO-11 +SAPO-31	Silica sol	na
		4		9.1	SAPO-31(r)	Silica sol	100
		6		9.6	SAPO-11 +SAPO-31	Silica sol	na
		10		9.5	SAPO-11	Silica sol	na

[a] Relative crystallinity (XRD) = (s) × 100/(r).
[b] na = not applicable.

was too slow (at 0.5 K min^{-1}) or produced materials with lower crystallinity (1.5 to 3 K min^{-1}). Subsequently, the autoclave was quenched, the products filtered, washed with distilled water, dried at 383 K and finally calcined at 793 K for 8 h. SAPO-11, SAPO-5 and SAPO-31 materials were also prepared following procedures [10] reported previously, which involved placement of the autoclave directly into a preheated (473 K) oven.

X-ray powder diffraction (XRD) patterns were recorded on a Rigaku instrument (model D/Max-VC, Cu Kα radiation, nickel filter, $\lambda =$ 1.5404 Å). The relative crystallinities (%) of the samples synthesized by the different methods and for different crystallization periods were estimated by XRD by summing the areas of six major diffraction peaks in the 2θ region from 5° to 45°. Solid-state MAS NMR spectra were recorded on a Brucker MSL-300 spectrometer. ^{29}Si MAS NMR spectra were measured at a spinning speed of 2.3 kHz, spectral width of 20 kHz, pulse length of 2 ms, delay of 2 s and spectrometer frequency of 59.6 MHz; tetramethylsilane (TMS) was used as the external standard. ^{27}Al MAS NMR spectra

were measured at a spectral width of 125 kHz, pulse length of 1 ms, delay of 500 ms and spectrometer frequency of 78.2 MHz using $Al(H_2O)_6^{3+}$ in a nitric acid solution of $Al(NO_3)_3$ as the external standard. The size and the morphology of the samples were examined by scanning electron microscopy (Leica Stereoscan 440 model; M/S Leica Cambridge Ltd, UK). The surface areas according to the Brunauer–Emmett–Teller (BET) method were determined by using a volumetric adsorption apparatus (model Omnisorb, 100CX; Coulter, USA). The acidities of the calcined SAPO-11 and SAPO-31 samples were determined by temperature-programmed desorption of pyridine using the procedure [13] reported previously.

Isomerization of *m*-xylene and alkylation of toluene with methanol were carried out in a fixed-bed, down-flow, tubular glass reactor at atmospheric pressure over the calcined samples. The catalyst powder was pelletized, sieved to 10–20 mesh size and a 2 g quantity was loaded in the reactor. The catalyst was activated at 823 K in air and flushed in N_2 before each run. The reactant was fed with a syringe pump (Sage Instruments, USA) (Weight Hourly Space Velocity, WHSV = 3 h^{-1}). The products of the reaction were collected downstream from the reactor in a cold trap (0°C) and analysed by a gas chromatograph (Shimadzu; Bentone column, FID detector) at different time intervals.

3. Results and discussion

3.1. Synthesis

Some typical results of the crystallization kinetics are given in Table 1. Experiments 1 and 2 (method 1) refer to the synthesis of SAPO-11 and SAPO-31 using DPA and fumed silica, following the conventional heating procedure of placing the autoclave inside an oven preheated to the desired temperature. As SAPO-5 was not crystallizable with DPA by the above procedure, triethylamine was used for its synthesis (Table 1, experiment no. 3). Experiments 4 to 12 (method 2) were carried out by crystallization using a slow and programmed heating of the autoclave to 473 K as described in the Experimental section. The interesting aspect of this synthesis is the crystallization of pure SAPO-5 using DPA as the template. This confirms the earlier conclusions of Ojo and McCusker [2] that DPA favours the formation of straight channels. The experiments reveal that the nature of the crystalline phase obtained and its purity depend on the pH of the gel and the source of SiO_2. Very interestingly, the crystalline product was obtained within a few hours of attaining the crystallization temperature (473 K). This reduces the overall crystallization time significantly, which is an advantage when synthesizing large volumes of SAPOs for commercial applications. It was observed that, while at SiO_2 contents between 0.3 and 0.4 mol both SAPO-5 and SAPO-11 were obtained as mixed phases (Table 1, experiments 6 and 7), at a SiO_2 content of 0.4 mol SAPO-5 was obtained as a pure phase only at pH = 6.8 (Table 1, experiment no. 8), above which mixed SAPO-5 and SAPO-11 phases were obtained. But at a SiO_2 molar ratio of 0.6–0.8, SAPO-5 was obtained as a pure phase over a wider pH range, 6.8–7.1 (Table 1, experiments 9, 10 and 11). So it is concluded that SAPO-5 could be obtained as a pure phase over a wide pH range using DPA as the template only when the SiO_2 molar ratio is >0.4. SiO_2 is found to have a promoting as well as a stabilizing effect on the $AlPO_4$-5 structure. The X-ray crystallinity of the SAPO-5 sample increased with increasing silicon content and was maximum at an SiO_2 content of 0.6 mol in the gel (Table 1, experiments 8, 9, 10 and 11).

Table 2 shows that, for the same SiO_2 content in the gel (0.2 molar ratio), the silicon content of the product was higher for the samples synthesized by programmed heating of the gel (method 2). Also, for the SAPO-5 samples, the crystallization time for the most crystalline sample was found to be lower for samples with higher silicon content. During the synthesis of SAPO-5, the phase purity of the sample was not much sensitive to the pH of the gel at a high SiO_2 content of 0.6–0.8 mol (Table 1, experiments 9, 10 and 11), but it was very much sensitive to pH at lower SiO_2 content (Table 1, experiments 4, 5, 6, 7 and 8). Under many conditions (Table 1) both SAPO-5 and

Table 2
Physicochemical properties of the samples

Experiment no.[a]	Sample	Product composition	Particle size (μm)	Particle shape	Surface area (m² g⁻¹)	Pyridine desorbed[b] (μmol g⁻¹)
1	SAPO-11(s)	$(Al_{0.57}P_{0.38}Si_{0.05})O_2$	∼5.0	Spherical	140	59.0
4	SAPO-11(r)	$(Al_{0.58}P_{0.35}Si_{0.07})O_2$	1.0×0.5	Rectangular	208	98.0
2	SAPO-31(s)	$(Al_{0.56}P_{0.41}Si_{0.03})O_2$	$(2.0–6.0) \times 1.0$	Rectangular rod	207	69.3
7	SAPO-31(r)	$(Al_{0.55}P_{0.39}Si_{0.06})O_2$	3.5×1.0	Rhombohedral	218	121.0
3	SAPO-5(s)	$(Al_{0.45}P_{0.46}Si_{0.09})O_2$	5.0–8.0	Mixed	153	–
9	SAPO-5(r)	$(Al_{0.50}P_{0.39}Si_{0.11})O_2$	6.0×8.0	Hexagonal prism	182	–

[a] As in Table 1.
[b] Beyond 573 K.
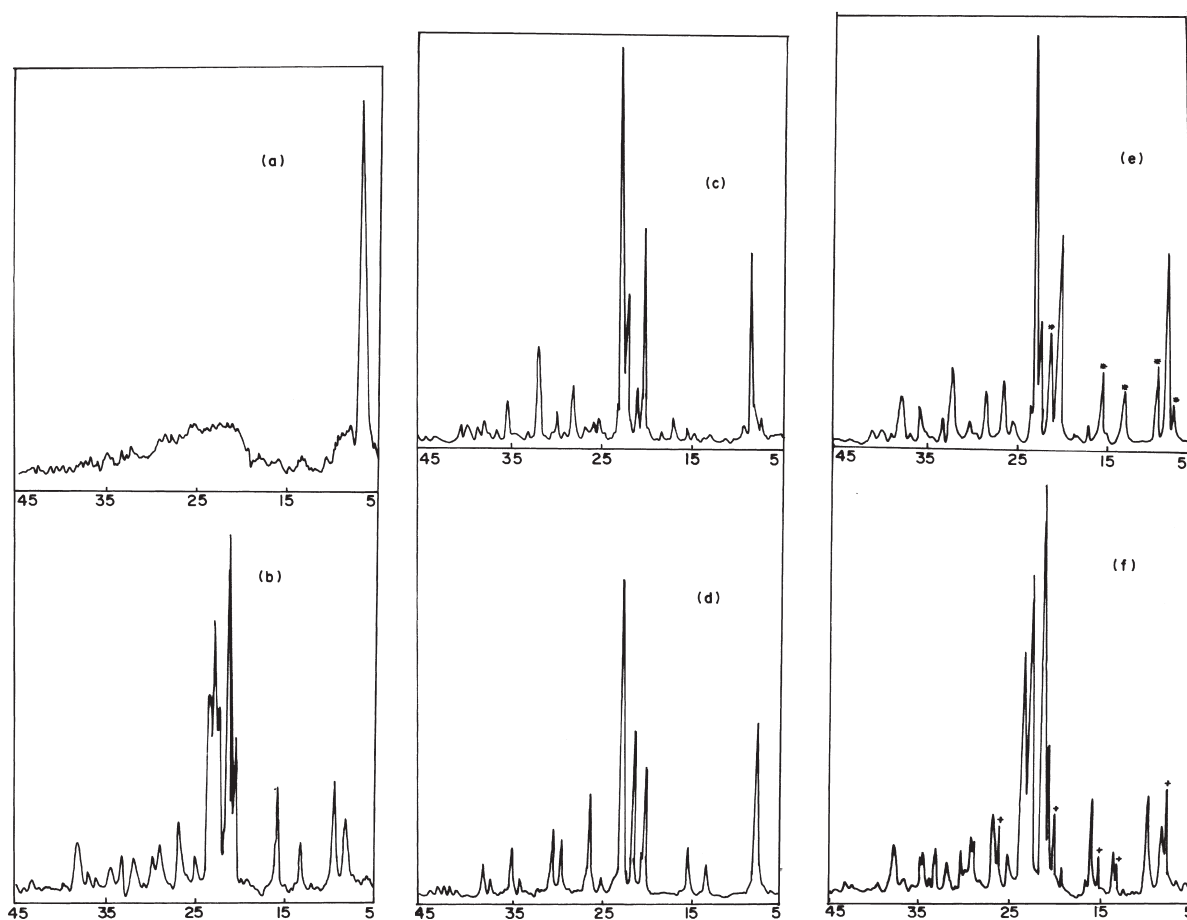
Fig. 1. XRD patterns of: (a) lamellar phase (experiment no. 12); (b) SAPO-11 (experiment no. 4); (c) SAPO-31 (experiment no. 12); (d) SAPO-5 (experiment no. 9); (e) SAPO-11+SAPO-31 (where ∗ denotes SAPO-11 peaks, experiment no. 12); and (f) SAPO-11+SAPO-5 (where + denotes SAPO-5 peaks, experiment no. 5).
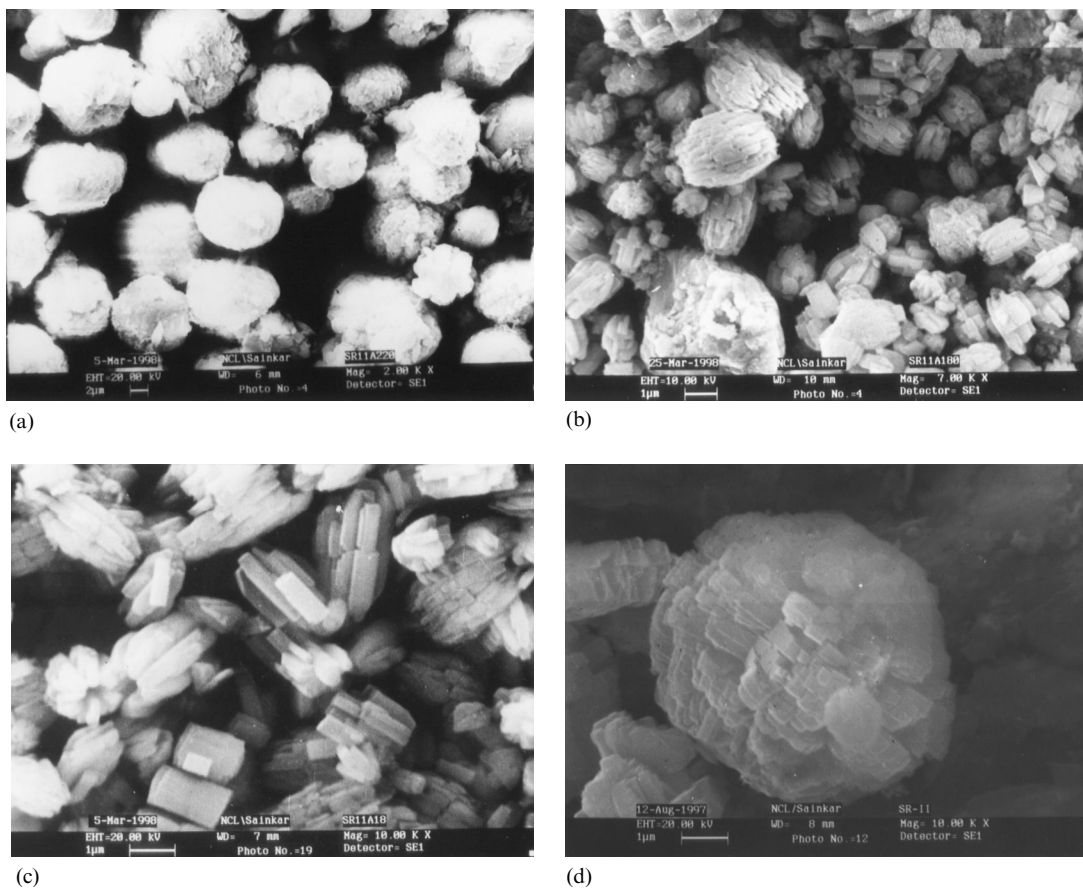
(a)

(b)

(c)

(d)

Fig. 2. SEM micrographs of: (a) SAPO-11(s) (experiment no. 1); (b) SAPO-11(r), 0 h (experiment no. 4); (c) SAPO-11(r), 2 h (experiment no. 4); (d) SAPO-11(r), 6 h (experiment no. 4); (e) SAPO-31(s) (experiment no. 2); (f) SAPO-31(r) (experiment no. 12); (g) SAPO-5(s) (experiment no. 3); (h) SAPO-5(r) (experiment no. 9); and (i) lamellar phase (experiment no. 12).

SAPO-11 co-crystallize and there was no phase transformation of one into the other even when crystallization was carried out for 12 h. SAPO-5, being the structure of higher simplicity, crystallized easily over a wider range of synthesis conditions than SAPO-11. It was also observed that when the gel (Table 1, experiment no. 6) for SAPO-5 synthesis was heated to 443 K at the rate of 1.5 K min^{-1} and kept at 443 K for 1 h, then a lamellar phase with an intense peak at $2\theta = \sim 6.8°$ was observed.

When silica sol was used instead of fumed silica and the gel pH was 6.5 (Table 1, experiment no. 7), a precursor phase similar to the one found in the case of SAPO-5 with a very intense peak at

$2\theta = \sim 6.8°$ was observed. This is probably a short-range ordered lamellar-type aluminophosphate phase. The formation of similar precursor lamellar phases during the synthesis of AlPO$_4$s and SAPOs has already been reported [14]. After 2 h crystallization time, SAPO-11 with SAPO-31 as impurity phase was observed, which transformed into pure SAPO-31 phase after 4 h of crystallization time. There was a further transformation into pure SAPO-11 after crystallization for 10 h. This successive phase transformation can be written as lamellar→SAPO-11+SAPO-31→SAPO-31→SAPO-11+SAPO-31→SAPO-11. A similar phase transformation has been recently reported by Lopez et al. [15].
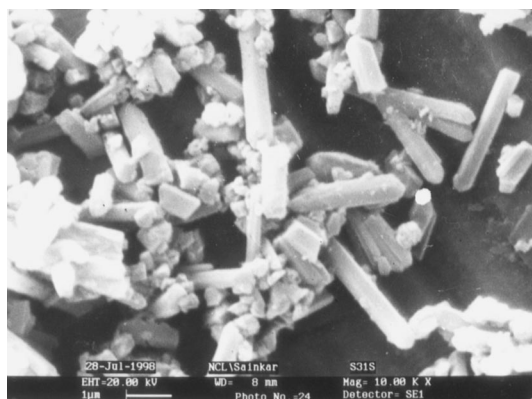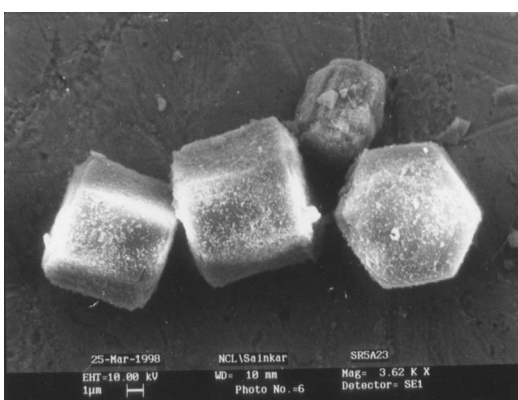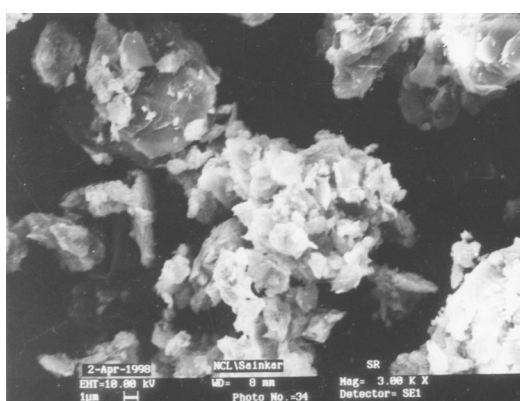
(e)
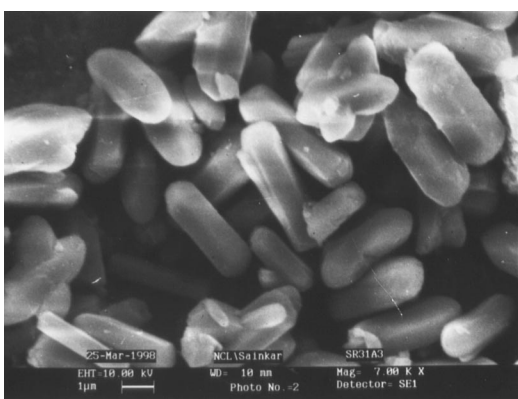
(f)
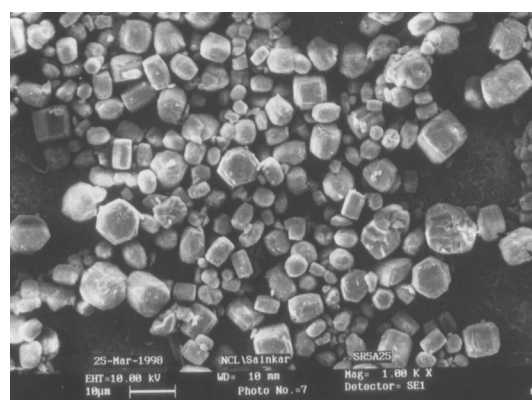
(g)

(h)

(i)

Fig. 2. (**continued**)

3.2. Characterization

Fig. 1(a)–(f) show the XRD patterns of the lamellar phase obtained by method 2, SAPO-11, SAPO-31, SAPO-5, SAPO-11+SAPO-31 mixed phase and SAPO-11+SAPO-5 mixed phase, respectively. The XRD crystallinities of the samples synthesized by method 2 were much larger than those of the conventionally synthesized samples (method 1). Physicochemical properties of all the SAPOs are presented in Table 2. The surface areas of the rapidly crystallized samples (designated r; method 2) were higher than those of the conventionally synthesized samples (designated s; method 1), which is expected from the higher X-ray crystallinity of the former samples.

SAPO-11(s) consisted of crystallites aggregated into spheres [Fig. 2(a)]. In contrast, SAPO-11(r) was in the form of well-defined rectangular crystallites of size $1.0 \, \mu m \times 0.5 \, \mu m$ only partially aggregated into hollow spheroids [Fig. 2(c)]. This sample did not reveal any amorphous component even at a crystallization time of 0 h although the crystallite shape was not well defined [Fig. 2(b)]; they were more like irregular jarred elongated plates. After 6 h crystallization time, the crystallites were completely aggregated axially into spheres [Fig. 2(d)]. SAPO-31(s) was made up of rectangular rod-like crystals of various sizes in the range from $1.0 \, \mu m \times 0.5 \, \mu m$ to $3.0 \, \mu m \times 0.5 \, \mu m$ [Fig. 2(e)]. But the rapidly crystallized SAPO-31(r) sample consisted of particles of uniform rhombohedral shape and size ($3.0 \, \mu m \times 1.0 \, \mu m$) [Fig. 2(f)]. SAPO-5(s) had crystals of different morphologies [Fig. 2(g)], whereas SAPO-5(r) was made up of only hexagonal prism-shaped single crystals of $6.0 \, \mu m \times 8.0 \, \mu m$ size and no other type of morphology was found [Fig. 2(h)]. So, it is concluded that synthesis by method 2 results in particles with well-defined uniform morphology and particle size. The SEM micrograph of the lamellar phase revealed flake-like particles [Fig. 2(i)].

On the basis of various reports, Oliver et al. [16] recently proposed that the crystallization of most aluminophosphates presumably follows a chain-to-layer transformation process wherein the parent chain is initially hydrolysed in solution, leading to the formation of other chain structure types. Further, chain condensation causes cross-linking and leads to a porous layer or open-framework structure. Our observations during the synthesis of SAPOs by method 2 could be rationalized by the above mechanism. In the latter method, where the aluminophosphate precursor gel is gradually heated from room temperature to 473 K, the formation of the parent chain and the hydrolysis to other chain types followed by chain condensation take place slowly in consecutive steps with increasing temperature. In the conventional synthesis procedure (method 1) it is possible that, due to the rapid initial heating of the gel, all three steps overlap and the chain species have more difficulty in undergoing condensation so that not only is a longer crystallization time required for the realization of a porous structure (Fig. 3) but also the particle morphology and size are not uniform. In addition, the crystallinities of the samples are also lower when the heating rate is not controlled. SAPO-5, with the simplest structure, is fully crystallized when the gel reaches 473 K (at 0 h) while SAPO-11 and SAPO-31 crystallize fully only after the gel has been kept at 473 K for some time (Table 1). Furthermore, SAPO-5 could be crystallized over a broader range of synthesis conditions than SAPO-11 or SAPO-31, the last structure being most sensitive to parameter changes.

^{27}Al MAS NMR spectra of the SAPOs prepared by the two methods after calcination are shown in Fig. 4. All the spectra consist of an intense peak at $\delta = \sim 39$ ppm typical of tetrahedral aluminium
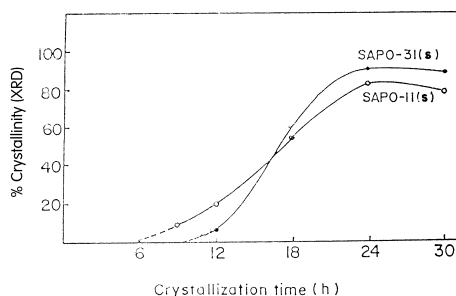

Fig. 3. Crystallization kinetics of SAPO-11(s) (experiment no. 1) and SAPO-31(s) (experiment no. 2).
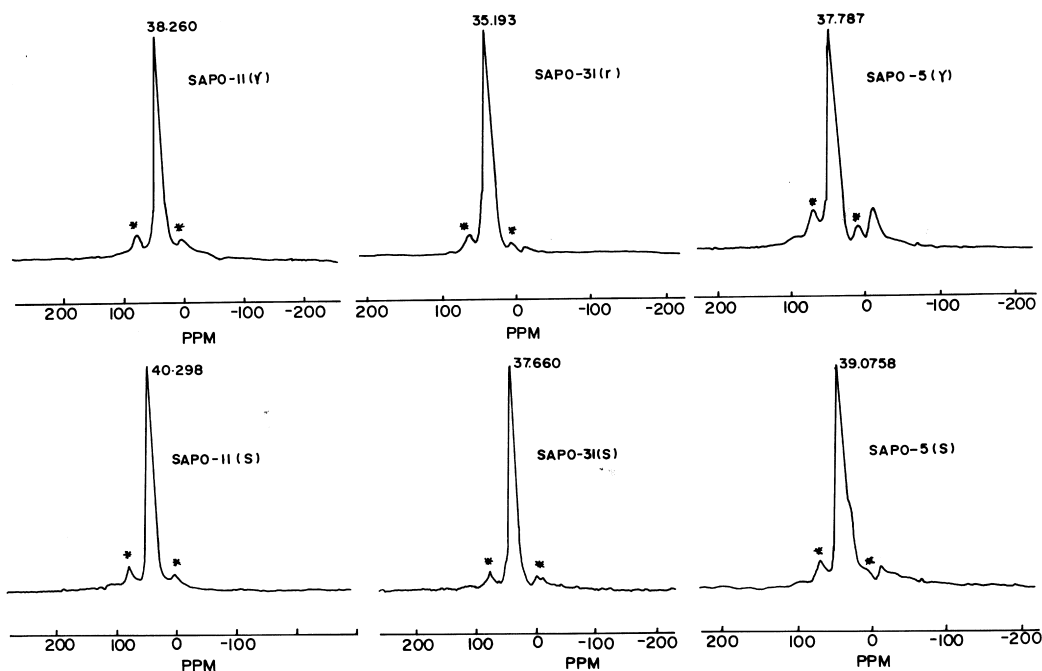
Fig. 4. ^{27}Al MAS NMR spectra of different SAPOs: SAPO-11(s) (experiment no. 1); SAPO-11(r) (experiment no. 4); SAPO-31(s) (experiment no. 2); SAPO-31(r) (experiment no. 12); SAPO-5(s) (experiment no. 3); and SAPO-5(r) (experiment no. 9) (where * denotes spinning side bands).

in the framework. Low-intensity peaks at around $\delta = -8$ and -12 ppm are found for all the samples, attributable to pentacoordinated and hexacoordinated aluminium [17–19] resulting from the coordination of tetrahedral framework aluminium with water molecules.

^{29}Si MAS NMR spectra of the samples synthesized by the two methods are shown in Fig. 5. The conventionally synthesized samples show a broad band in the region of $\delta = -90$ to -110 ppm, indicating the presence of large amounts of multiple silicon environments and the formation of siliceous islands. The rapidly crystallized samples, on the other hand, exhibit a very intense peak at about $\delta = -95$, -89 and -90 ppm for SAPO-11, SAPO-31 and SAPO-5 samples, respectively, with lower-intensity signals in the $\delta = -100$ to -110 ppm region. This indicates that a large amount of the silicon is present as Si(4Al)-type species in the framework and that there is minimal

formation of silicon-containing islands in the samples synthesized by method 2.

3.3. Catalytic activity

Studies of the isomerization of m-xylene carried out over the samples (Table 3) reveal a higher catalytic activity for the samples synthesized by the rapid crystallization method. This can be attributed to the higher surface area and to maximum incorporation of silicon at phosphorus sites, resulting in fewer silicon islands and more isolated silicon species (as evidenced from ^{29}Si MAS NMR) and thus leading to more Brønsted acid sites. The total acidity of the samples synthesized by method 2 was also found experimentally to be greater (Table 2). These samples desorbed more pyridine beyond 573 K than the conventional samples (s). The isomerization-to-disproportionation (I/D) ratios are higher for the rapidly crystallized
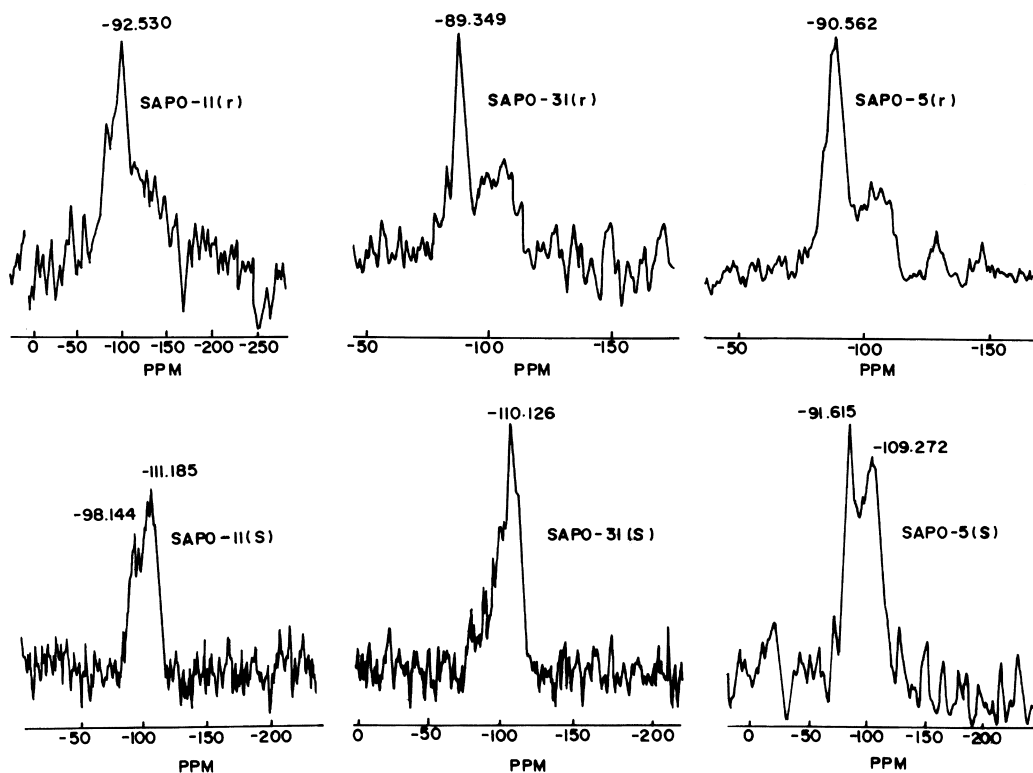
Fig. 5. ^{29}Si MAS NMR spectra of different SAPOs: SAPO-11(s) (experiment no. 1); SAPO-11(r) (experiment no. 4); SAPO-31(s) (experiment no. 2); SAPO-31(r) (experiment no. 12); SAPO-5(s) (experiment no. 3); and SAPO-5(r) (experiment no. 9).

Table 3
m-Xylene isomerization over different samples (conditions: reaction temperature = 623 K; time on stream = 3 h; WHSV = 3 h^{-1})

Catalyst	Conversion (wt%)	Product distribution (wt%)				p-Xylene/o-xylene	I/D
		Benzene	Toluene	p-Xylene + o-xylene	TMB[a]		
SAPO-11(r)	14.7	–	0.2	14.17	0.28	2.0	29.5
SAPO-11(s)	9.4	–	0.38	8.66	0.36	2.2	11.8
SAPO-31(r)	13.2	–	0.50	12.22	0.48	1.4	12.6
SAPO-31(s)	7.8	–	0.59	6.58	0.63	1.5	5.2
SAPO-5 (r)	73.29	1.2	19.86	30.74	20.89	1.05	0.73
SAPO-5 (s)	66.51	0.5	18.08	28.87	19.56	1.05	0.77

[a] TMB = trimethylbenzenes.

samples of SAPO-11 and SAPO-31. The higher disproportionation activity of the conventional samples is probably due to the presence of some very strong acid sites due to silicon atoms at the edges of silicon islands [10] and to SiO_2–Al_2O_3 phases present in them. In the case of SAPO-5, the I/D ratios are similar for the samples synthe-

sized by the two methods. The higher conversions and small I/D ratios in SAPO-5 samples are probably due to both the larger pore size (~ 7 Å) and the higher silicon contents in these samples. Toluene alkylation over the various samples also shows a much higher activity for the samples synthesized by the rapid crystallization method

Table 4
Toluene alkylation over different samples (conditions: reaction temperature = 623 K; time on stream = 3 h; WHSV = 3 h^{-1})

Catalyst	Conversion (wt%)	Product distribution (wt%)					p-Xylene/total xylene
		Benzene	p-Xylene	m-Xylene	o-Xylene	Total TMB[a]	
SAPO-11(r)	32.42	0.3	16.45	8.21	3.58	3.87	0.58
SAPO-11(s)	11.72	0.3	6.5	2.86	1.22	0.79	0.61
SAPO-31(r)	36.58	0.34	17.08	9.16	3.98	5.53	0.57
SAPO-31(s)	16.96	0.04	7.84	4.83	2.50	1.74	0.52
SAPO-5(s)	20.98	0.73	4.06	3.55	6.49	6.14	0.29
SAPO-5(r)	29.69	2.01	6.31	7.33	8.11	5.89	0.29

[a] TMB = trimethylbenzenes.

(Table 4). Studies of both *m*-xylene isomerization and toluene alkylation do not reveal any differences in shape-selectivity effects between the samples synthesized by the two methods.

4. Conclusions

Gradual and controlled heating of the silicoaluminophosphate precursor gel to the required temperature results in the formation of highly crystallized SAPOs in a short time. SAPO-5 crystallizes at high silicon content (0.4–0.6 mol SiO$_2$) and high pH (6.9–7.1), while SAPO-11 crystallizes at a lower silicon content (0.1–0.3 mol SiO$_2$) and a pH of ~6.8. Using silica sol instead of fumed silica results in SAPO-31 after a crystallization time of 4 h, which transforms to SAPO-11 after a crystallization time of 10 h. Rapid crystallization results in particles of uniform size and morphology with the incorporation of silicon preferentially at phosphorus sites. As a result, the samples show much higher activity (and selectivity) in the isomerization of *m*-xylene and the alkylation of toluene.

References

[1] E.M. Flanigen, R.L. Patton, S.T. Wilson, in: P.J. Grobet, W.J. Mortier, E.F. Vansant, G. Schulz-Ekloff (Eds.), Innovation in Zeolite Material Science, Elsevier, Amsterdam, 1988, p. 13.
[2] A.F. Ojo, L.B. McCusker, Zeolites 11 (1991) 460.
[3] S.T. Wilson, B.M. Lok, C.A. Messina, E.M. Flanigen, in: ACS Symposium Series vol. 218, American Chemical Society, Washington, DC, 1983, p. 79.
[4] S.T. Wilson, B.M. Lok, C.A. Messina, E.M. Flanigen, in: Proceedings of the Sixth International Zeolite Conference, Butterworths, Guildford, 1985, p. 97.
[5] N.J. Tapp, N.B. Milestone, D.M. Bibby, Zeolites 8 (1988) 183.
[6] S.J. Miller, Microporous Mater. 2 (1994) 439.
[7] J.M. Campelo, F. Lafont, J.M. Marinas, Zeolites 15 (1995) 97.
[8] J.M. Campelo, F. Lafont, J.M. Marinas, J. Catal. 156 (1995) 11.
[9] P. Meriaudeau, V.A. Tuan, V.T. Nghiem, S.Y. Lai, L.N. Hung, C. Naccache, J. Catal. 169 (1997) 55.
[10] B.M. Lok, C.A. Messina, R.L. Patton, R.T. Gajek, T.R. Cannan, E.M. Flanigen, US Patent No. 4 440 871, 1984.
[11] D. Barthomeuf, Zeolites 14 (1994) 394.
[12] M. Derewinski, M.J. Peltre, M. Briend, D. Barthomeuf, P.P. Man, J. Chem. Soc., Faraday Trans. 89 (11) (1993) 1823.
[13] V.R. Chowdhary, V.S. Nayak, Appl. Catal. A: Gen. 4 (1983) 31.
[14] N. Venkatathri, S.G. Hegde, V. Ramaswamy, S. Sivasanker, Microporous Mesoporous Mater. 23 (1998) 277.
[15] C.M. Lopez, F.J. Machado, J. Goldwasser, B. Mendez, K. Rodriguez, M.M.R. Agudelo, Zeolites 19 (1997) 133.
[16] S. Oliver, A. Kuperman, G.A. Ozin, Angew. Chem. Int. Ed. 37 (1998) 46.
[17] E. Jahn, D. Müller, W. Wieker, J. Richter-Mendau, Zeolites 9 (1989) 177.
[18] R. Jelinek, B.F. Chmelka, Y. Wu, M.E. Davis, J.G. Ulan, R. Gronsky, A. Pines, Catal. Lett. 15 (1992) 65.
[19] Y. Kustanovich, D. Goldfarb, J. Am. Chem. Soc. 95 (1991) 8818.